 doi:10.20944/preprints202009.0527.v1

Article

Study on Two-Phase Fluid-Solid Coupling Characteristics in Local-Saturated Zone of Subgrade Considering the Effect of Fine Particles Migration

Yu Ding [1,*], Jia-sheng Zhang [1,2], Yu Jia [1,*], Xiao-bin Chen [1,2], Xuan Wang [1,2] and Fei Meng [3]

[1] School of Civil Engineering, Central South University, Changsha, Hunan 410083, China; zjsdj@csu.edu.cn (J.-s.Z.); chen_xiaobin@csu.edu.cn (X.-B.C.); dddebug@csu.edu.cn (X.W.)

[2] MOE Key laboratory of Engineering Structures of Heavy Haul Railway, Central South University, Changsha, Hunan 410083, China

[3] Faculty of Science, Engineering and Technology, Swinburne University of Technology, Melbourne, VIC 3122, Australia; fmeng@swin.edu.au

* Correspondence: ding_yu@csu.edu.cn (Y.D.); jia_yu@csu.edu.cn (Y.J.)

Abstract: The fluid seepage in local-saturated zone of subgrade promotes the migration of fine particles in the filler, resulting in the change of pore structure and morphology of the filler and the deformation of solid skeleton, which affects the fluid seepage characteristics. Repeatedly, the muddy interlayer, mud pumping and other diseases are finally formed. Based on the theory of two-phase seepage, the theory of porous media seepage, and the principle of effective stress in porous media, a two-phase fluid-solid coupling mathematical model in local-saturated zone of subgrade considering the effect of fine particles migration is established. The mathematical model is numerically calculated with the software COMSOL Multiphysics®, the two-phase seepage characteristics and the deformation characteristics of the solid skeleton in local-saturated zone of the subgrade are studied. The research results show that due to the continuous erosion and migration of fine particles in local-saturated zone of the subgrade, the volume fraction of fine particles first increases then decreases and finally becomes stable with the increase of time. And the volume fraction of fine particles for the upper part of the subgrade is larger than that for the lower part of the subgrade. The porosity, the velocity of fluid, the velocity of fine particles, and the permeability show a trend of increasing first and then stabilizing with time; the pore water pressure has no significant changes with time. The vertical displacement increase first and then decrease slightly with the increase of time, and finally tend to be stable. For a filler with a larger initial volume fraction of fine particles, the maximum value of the volume fraction of fine particles caused by fluid seepage is larger, and the time required to reach the maximum value is shorter. It can be concluded that in actual engineering, the volume fraction of fine particles in the subgrade filler should be minimized on the premise that the filler gradation meets the requirements of the specification.

Keywords: local-saturated zone of subgrade; fine particles migration; two-phase seepage characteristics; deformation characteristics; volume fraction of fine particles

1. Introduction

Filler for railway subgrade is mostly coarse-grained soil materials, mixed with a certain proportion of fine-grained soil, and have complex pore structure characteristics. When atmospheric precipitation, surface water or snow melt infiltrates into subgrade and fails to be discharged in time, the local area of the subgrade will be saturated. Under the action of external load, excess pore water pressure will be generated in local-saturated zone of the subgrade, and the dissipation of excess pore water pressure will form a high-impact transient fluid, which will drive fine particles to seepage in

the pores of the filler [1-3]. In the process of fluid seepage, there are complex effects of erosion and migration of fine particles, which will lead to the change of pore structure and morphology of the filler. At the same time, the action of external load and the change of the pore structure of the filler will cause deformation of the solid skeleton, which will further change the fluid seepage channel and affect the fluid seepage characteristics, and ultimately induce a series of diseases such as mud interlayer, mud pumping, and so on [4-5]. It is of great significance to deeply explore the fluid seepage characteristics and solid skeleton deformation characteristics considering the effect of fine particles migration and the change of hydraulic characteristics of coarse-grained soil to analyze the disaster-causing mechanism of the above diseases.

At present, there are many studies on the model of fine particles migration and the mechanism of fine particles migration both theoretically and experimentally, and have achieved fruitful results. J. F. Schijven [6] and R. Kretzschmar [7] have established a classical fine particles migration model including the conservation equation of fine particles quantity and the kinetic equation of deposition. S. A. Bradford et al. [8] proposed a fine particles migration model considering the effect of sedimentation and sieving. On the basis of the traditional deep filtration model, J. Zhao et al. [9] applied the law of mass conservation, and established a particles migration model that considers the influence factors of seepage reduction coefficient, the velocity reduction coefficient, the change of porosity, and the suspended particles capture probability. The research result of I. Alobaidi [4-5] showed that the saturated interlayer water inside subgrade produces excess pore water pressure under the action of cyclic loading, which causes the vertical seepage of the water and the liquefied fine particles. B. Kermani [10] believed that the excess pore water pressure generated inside subgrade under cyclic loading drives the migration of fine particles, and the migration velocity of fine particles was analyzed. D. Liu, J. P. Herzig and other scholars [11-15] studied the influence of fine particles concentration and particles size on the characteristics of fine particles migration in porous media. Q. S. Liu [16] conducted an experimental study on the migration-deposition characteristics of suspended particles with different sizes in porous media, and divided the migration-deposition types of suspended particles into three types: filter cake filter type, migration-deposition type and free movement type.

On the other hand, the current research on fluid-solid coupling characteristics has achieved rich research results. The coupling theory of water and soil (rock) was first used to solve the consolidation problem of soil. Terzaghi [17] studied the coupling phenomenon of fluid-solid deformation, and first proposed the concept of effective stress and established a one-dimensional consolidation model of soil. Subsequently, Biot [18-19] established a relatively complete three-dimensional consolidation theory. Since the establishment of Biot's three-dimensional consolidation theory, researchers have introduced different material constitutive relations and applied them to a wider range of fields. Zienkiewicz [20] considered nonlinear materials and proposed the generalized Biot formula on the basis of Biot's three-dimensional consolidation theory. In 1982, Savage and Bradok [21] extended the Biot's three-dimensional consolidation theory to anisotropic elastic porous media. Zimmer-manl [22] introduced the dimensionless parameters to express the coupling effect of seepage and stress, and further extended the theoretical model of the coupling of multiphase saturated seepage in porous media. In 1943, Z. J. Shen [23] first combined Biot's consolidation theory with finite element method and applied it to slope stability analysis. Y. Liang [24] obtained a fluid-solid coupling model of piping failure based on the mass conservation equation and the continuity equation of seepage. Z. Zhou [25] conducted artificial rainfall simulation tests on soil-rock mixture slopes, and studied the permeability of soil-rock mixture. On the basis of fluid mechanics and soil mechanics, W. Chen [26] derived the equilibrium equation of porous media and the continuity equation of pore fluid considering the coupling of stress field and seepage field, and established a fluid-solid coupling model.

However, the above researches on the characteristics of fine particles migration and fluid-solid coupling are mostly separate, and seldom involve the influence of fine particles migration on the hydraulic characteristics of coarse-grained soils. There is a lack of systematic research on the

Preprints (www.preprints.org) | NOT PEER-REVIEWED | Posted: 23 September 2020 doi:10.20944/preprints202009.0527.v1

coupling effect between fine particles migration, fluid seepage and deformation characteristics of solid skeleton.

Therefore, based on the theory of two-phase seepage, the theory of porous media seepage, and the principle of effective stress in porous media, this paper establishes a two-phase fluid-solid coupling mathematical model considering the effect of fine particles migration. The mathematical model is numeralized by the software COMSOL Multiphysics®. And the characteristics of fine particles migration, the two-phase seepage and the deformation of solid skeleton are studied.

2. Two-phase fluid-solid coupling mathematical model considering the effect of fine particles migration

2.1. Basic assumption

Filler for railway subgrade is mostly coarse-grained soil materials, mixed with a certain proportion of fine-grained soil, and have complex pore structure characteristics. Therefore, the saturated coarse-grained filler can be regarded as a saturated porous medium composed of solid medium (coarse particles and fine particles), fluid medium in pores, and fine particles that erode into the fluid medium that can migrate with the fluid (hereinafter referred to as fine particles). The structure of saturated porous media is shown in figure 1. In order to establish a two-phase fluid-solid coupling mathematical model in local-saturated zone of subgrade considering the effect of fine particles migration, the following assumptions are made:

(1) The coarse-grained filler is uniform and isotropic linear elastomer, and satisfies the assumption of small strain;

(2) The seepage of water in the pores is caused by the pore water pressure gradient and follows Darcy's law;

(3) The influence of temperature and chemical action on the properties of subgrade filler is not considered;

(4) Solid particles and water are incompressible;

(5) The movable fine particles are spheres with the same radius d_p, and the influence of fine particles on the fluid seepage characteristics and the force between fine particles are ignored.

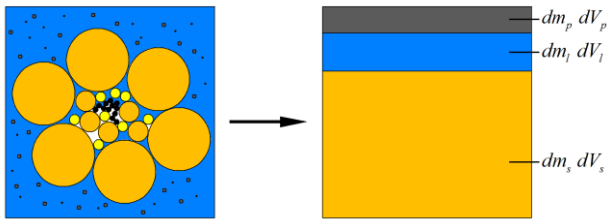

Figure 1. Micro-model for saturated porous medium (a) Micro-model; (b) Three-phase model.

2.2. Establishment of two-phase fluid-solid coupling mathematical model considering the effect of fine particles migration

2.2.1. Equations of seepage field

- (1) Basic definition

As shown in figure 1, the micro-model for coarse-grained soil is composed of three parts, which are solid medium (s, dm_s is mass of the solid and dV_s is volume of the solid), fluid medium (l, dm_l is mass of the solid and dV_l is volume of the solid), and fine particles (p, dm_p is mass of the solid and dV_p is volume of the solid).

Preprints (www.preprints.org) | NOT PEER-REVIEWED | Posted: 23 September 2020 doi:10.20944/preprints202009.0527.v1

Porosity of porous media is defined as:

$$\phi = \frac{dV_V}{dV} = \frac{dV_l + dV_p}{dV} \tag{1}$$

where: ϕ is the porosity of the micro-model; dV_V is the pore volume of the micro-model (m^3); dV is the total volume of the micro-model (m^3).

The volume fraction of fine particles is:

$$C = \frac{dV_p}{dV_V} \tag{2}$$

where: C is the volume fraction of fine particles.

- (2) Equations of mass conservation

According to the law of mass conservation of fluid, when considering the two-phase (fluid and fine particles) seepage in porous media, the mass conservation equations of fluid phase and fine particles phase can be expressed as:

$$\frac{\partial}{\partial t}[\phi(1-C)\rho_l] + \nabla[(1-C)\rho_l v_{ls}] = q_l \tag{3}$$

$$\frac{\partial}{\partial t}(\phi C \rho_p) + \nabla(C\rho_p v_{ps}) = \dot{m} \tag{4}$$

where: ρ_l is the inherent density of the fluid ($\mathrm{kg/m^3}$); ρ_p is the inherent density of fine particles ($\mathrm{kg/m^3}$); v_{ls} is the velocity vector of the fluid relative to the solid ($\mathrm{m/s}$); q_l is the source (sink) item of the fluid ($\mathrm{kg/m^3 s}$); v_{ps} is the velocity vector of fine particles relative to solid ($\mathrm{m/s}$); $\dot{m}$ is the mass rate of fine particles migration ($\mathrm{kg/m^3 s}$); $\nabla = \frac{\partial}{\partial x}\mathbf{i} + \frac{\partial}{\partial y}\mathbf{j} + \frac{\partial}{\partial z}\mathbf{k}$ is Hamiltonian operator.

- (3) Equations of motion

The seepage of fluid conforms to Darcy's law, as follows:

$$v_{ls} = v_l - v_s = -\frac{k}{\mu_l}(\nabla p_l - \rho_l g) \tag{5}$$

where: v_l is the velocity vector of the fluid ($\mathrm{m/s}$); v_s is the velocity vector of solid ($\mathrm{m/s}$); k is the permeability of porous media ($\mathrm{m^2}$); p_l is the pore pressure of the fluid (Pa); μ_l is the dynamic viscosity coefficient of the fluid ($\mathrm{Pa \cdot s}$); g is the gravitational acceleration vector ($\mathrm{N/kg}$).

The force of fine particles in liquid is complex. The fine particles is mainly affected by effective gravity, drag force, additional mass force, pressure gradient force, Basset force, Magnus force, Saffman force and other force, among which additional mass force and pressure gradient force, Basset force, Magnus force, Saffman force have relatively small influence on the movement of fine particles and can be ignored. Therefore, considering the effect of effective gravity and drag force on fine particles, the schematic diagram of the force on a single fine particle is shown in figure 2.

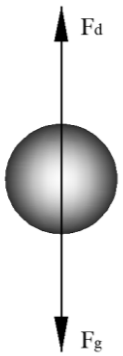

Preprints (www.preprints.org) | NOT PEER-REVIEWED | Posted: 23 September 2020 doi:10.20944/preprints202009.0527.v1

Figure 2. The schematic diagram of the force on a single fine particle.

We use v_r to represent the difference between the velocity vector of the fluid and the velocity vector of the fine particles (v_p). Assuming that the velocity of the fine particles differs little from that of fluid in the horizontal direction, and the velocity difference in the vertical direction can be expressed as:

$$v_{rz}=v_{lz}-v_{pz} \tag{6}$$

When a single particle is in force equilibrium in the fluid, there are:

$$(\rho_p-\rho_l)\frac{\pi d_p^3}{6}g=C_D\frac{\pi d_p^2}{4}\frac{\rho_l v_{rz}^{\ 2}}{2} \tag{7}$$

then:

$$v_{rz}=\sqrt{\frac{4(\rho_p-\rho_l)d_p g}{3C_D\rho_l}} \tag{8}$$

where, d_p is the diameter of fine particles (m); C_D is the coefficient of drag force, which is related to the Reynolds number of fine particles.

$$\mathrm{Re}=\frac{d_p\rho_l u_l}{\mu_l} \tag{9}$$

$$\begin{cases} C_D=\dfrac{24}{\mathrm{Re}}, & \mathrm{Re}<2,\ \text{Laminar flow zone;} \\ C_D=\dfrac{18.5}{\mathrm{Re}^{0.6}}, & 2<\mathrm{Re}<500,\ \text{Transition zone;} \\ C_D\approx 0.44, & 500<\mathrm{Re}<2\times10^5,\ \text{Turbulence zone;} \\ C_D\approx 0.11, & \mathrm{Re}>2\times10^5,\ \text{Turbulent boundary zone;} \end{cases} \tag{10}$$

According to Equations (6) ~ (10), the motion equations of fine particles can be obtained:

$$\begin{cases} v_{psx}=-\dfrac{k}{\mu_l}\dfrac{\partial p_l}{\partial x} \\ v_{psy}=-\dfrac{k}{\mu_l}\dfrac{\partial p_l}{\partial y} \\ v_{psz}=-\dfrac{k}{\mu_l}\left(\dfrac{\partial p_l}{\partial z}-\rho_l g\right)-\sqrt{\dfrac{4(\rho_p-\rho_l)d_p g}{3C_D\rho_l}} \end{cases} \tag{11}$$

2.2.2. Equations of stress field

According to the principle of effective stress in saturated porous medium, there are:

$$\sigma_{ij}=\sigma'_{ij}+\phi p_l\delta_{ij} \tag{12}$$

where, σ_{ij} is the total stress tensor; σ'_{ij} is the effective stress tensor; δ_{ij} is the Kronecker symbol, $\delta_{ij}=\begin{cases}1, i=j\\0, i\neq j\end{cases}$.

According to the assumption that the solid skeleton is uniform and isotropic linear elastomer, and satisfies the assumption of small strain, its constitutive equation is:

$$\sigma'_{ij}=\lambda\varepsilon_V\delta_{ij}+2\mu\varepsilon_{ij} \tag{13}$$

Preprints (www.preprints.org) | NOT PEER-REVIEWED | Posted: 23 September 2020 doi:10.20944/preprints202009.0527.v1

where, ε_V is the volumetric strain of the solid skeleton, $\varepsilon_V=\varepsilon_x+\varepsilon_y+\varepsilon_z$, and $\varepsilon_x,\varepsilon_y,\varepsilon_z$ is the axial strain in the three directions of x, y and z, respectively; ε_{ij} is the strain of the solid skeleton; λ、μ is the constant of Lamé,

$$\lambda=\frac{Ev}{(1+v)(1-2v)} \tag{14}$$

$$\mu=\frac{E}{2(1+v)} \tag{15}$$

where, E is Young's elastic modulus; v is Poisson's ratio.

The displacement of the solid skeleton is expressed in terms of u_s, and the relation between strain and displacement is:

$$\varepsilon_{ij}=\frac{1}{2}(u_{sj,i}+u_{si,j}) \tag{16}$$

Then, the stress balance equation of porous media can be expressed as:

$$\sigma_{ij,j}+R_i=0 \tag{17}$$

where, R_i is the volume force of the porous medium (N);

$$R_i=\rho g=[(1-\phi)\rho_s+\phi(1-C)\rho_l+\phi C\rho_p]g \tag{18}$$

where, ρ is the average density of the porous medium ($\mathrm{kg/m^3}$); ρ_s is the inherent density of the solid ($\mathrm{kg/m^3}$).

Then, the governing equation of the stress field of porous media can be obtained from equations (12), (13), (16), (17) and (18).

$$(\lambda+\mu)\nabla\varepsilon_V+\mu\nabla^2u_{si}+\nabla(\phi p_l\delta_{ij})+R_i=0 \tag{19}$$

2.2.3. Migration equation of fine particles

According to the references [27-30], considering the limit value of the migration of fine particles [31-34]. The migration equation of fine particles is as follows:

$$\dot{m}=\rho_p\zeta(\phi_{\max}-\phi)(C-\frac{C^2}{C_{cr}})|v_l| \tag{20}$$

where: $\phi_{\max}$ is the maximum porosity, which refers to the limit value of porosity change in porous media caused by the migration of fine particles; C_{cr} is the critical volume fraction of fine particles when the migration reach equilibrium; $|v_l|$ is the modulus of the velocity vector of the fluid ($\mathrm{m/s}$); ζ is the erosion coefficient of fine particles ($\mathrm{m^{-1}}$).

2.2.4. Auxiliary equation

- (1) Porosity evolution equation

The change in pore volume is mainly caused by the erosion and migration of fine particles and the deformation of solid skeleton. For the erosion and migration of fine particles, the rate of change in pore volume is equal to the volume of erode fine particles per unit time, then:

$$\frac{\partial(dV_V)}{\partial t}=\frac{\dot{m}dV}{\rho_p} \tag{21}$$

which can be simplified as:

$$\frac{\partial\phi}{\partial t}=\frac{\dot{m}}{\rho_p} \tag{22}$$

Preprints (www.preprints.org) | NOT PEER-REVIEWED | Posted: 23 September 2020 doi:10.20944/preprints202009.0527.v1

For pore volume change caused by deformation of solid skeleton, the porosity equation proposed in reference [35] is as follows:

$$\phi = \frac{\phi_0 + \varepsilon_V}{1 + \varepsilon_V} \tag{23}$$

where, ϕ_0 is the initial porosity.

Equation (23) can be written as:

$$\frac{\partial \phi}{\partial t} = \frac{1 - \phi_0}{(1 + \varepsilon_V)^2} \frac{\partial \varepsilon_V}{\partial t} \tag{24}$$

Then, based on the erosion and migration of fine particles and the deformation of solid skeleton, the porosity evolution equation can be expressed as:

$$\frac{\partial \phi}{\partial t} = \frac{\dot{m}}{\rho_p} + \frac{1 - \phi_0}{(1 + \varepsilon_V)^2} \frac{\partial \varepsilon_V}{\partial t} \tag{25}$$

- (2) Relationship between permeability and porosity

The Kozeny-Carman equation was used to describe the relationship between permeability and porosity:

$$k = k_0 (\frac{\phi}{\phi_0})^3 (\frac{1 - \phi_0}{1 - \phi})^2 \tag{26}$$

where: k_0 is the initial permeability (m^2).

Equations (3) ~ (5), (11), (19), (20), (25), (26), constitute the two-phase fluid-solid coupling mathematical model considering the effect of fine particles migration.

2.2.5. Boundary conditions and initial conditions

The coupling mathematical model mentioned above is highly nonlinear, boundary conditions and initial conditions need to be given in the process of solution. The pore water pressure, the volume fraction of fine particles and the displacement of solid skeleton are taken as basic variables.

Boundary conditions: the boundary conditions usually have the first type, also known as Dirichlet boundary; and the second type, also known as Neumann boundary.

The first boundary conditions can be expressed as:

$$p_l = \bar{p}_l \quad \text{on} \quad \Gamma_{p_l};$$
$$C = \bar{C} \quad \text{on} \quad \Gamma_C;$$
$$u_s = \bar{u}_s \quad \text{on} \quad \Gamma_{u_s}.$$

The second boundary conditions can be expressed as:

$$q_l = -v_{ls} \cdot n \quad \text{on} \quad \Gamma_{q_l};$$
$$q_C = -C v_{ps} \cdot n \quad \text{on} \quad \Gamma_C;$$
$$\sigma_{ij} \cdot n = \bar{t} \quad \text{on} \quad \Gamma_{\sigma_{ij}}.$$

Initial conditions:

$$p_l = p_l^0, \; C = C^0, \; u_s = u_s^0 \quad \text{at} \quad t=0.$$

2.2.6. The solution of the mathematical model

Preprints (www.preprints.org) | NOT PEER-REVIEWED | Posted: 23 September 2020 doi:10.20944/preprints202009.0527.v1

The above mathematical model was solved by using the coupling solid mechanics module and porous medium multiphase flow module in the software COMSOL Multiphysics®. Take the volume fraction of fine particles (C), the pore pressure of the fluid (p_l), and the displacement of the solid skeleton (u_s) as the basic unknowns, and other unknowns such as the velocity vector of the fluid v_l, the velocity vector of the fine particles (v_p), the mass rate of fine particles migration ($\dot{m}$), the porosity (ϕ), and the permeability (k_0) can be can be calculated by the basic unknowns.

3. Validation of the coupling model

In this section, the software COMSOL Multiphysics® is used to solve the mathematical model. Moreover, the solution results were compared with those in reference [29] to verify the accuracy of the coupling model in this paper.

3.1. The establishment of numerical model

Reference [29] studied the problem of sand production in the wellbore during oil extraction. A two-dimensional calculation model is adopted. The radius of the wellbore (inner boundary) is 0.1m, and the outer boundary is 5m. The calculation model is shown in figure 3.

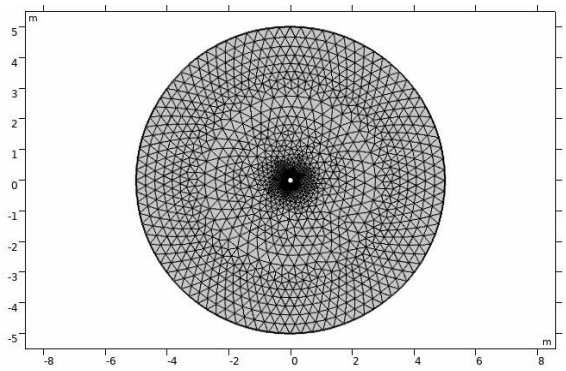

Figure 3. Illustration of wellbore erosion.

In this paper, the standard atmospheric pressure value is taken as the calculation reference value. The initial porosity of the model was 0.25, and the initial volume fraction of fine particles was 0.001. The boundary conditions adopted by the model are as follows: the fluid pressure at inner boundary is 5MPa, and the fluid pressure at outer boundary is 8MPa. The inner boundary is the outflow boundary for fine particles, and the external stress acting on the outer boundary is 20 MPa. The physical parameters are shown in Table 1.

Table 1. Physical parameters for numerical calculation.

Parameter	Value
Wellbore(inner boundary) radius r_a /(m)	0.1
Outer boundary radius r_o /(m)	5.0
Initial porosity ϕ_0	0.25
Maximum porosity ϕ_{max}	1
Initial volume fraction of fine particles C_0	1.0×10^{-3}
Critical volume fraction of fine particles C_{cr}	0.30
Initial permeability k_0 /(m^2)	3.73×10^{-13}

Preprints (www.preprints.org) | NOT PEER-REVIEWED | Posted: 23 September 2020 doi:10.20944/preprints202009.0527.v1

The dynamic viscosity coefficient of the fluid μ_l /(Pa·s)	4.2×10^{-3}
The density of fluid ρ_l /(kg/m^3)	1000
The density of fine particles ρ_p /(kg/m^3)	2650
The erosion coefficient of fine particles ζ /(m^{-1})	5.0
Fluid pressure at inner boundary p_{l-a} /(MPa)	5.0
Fluid pressure at outer boundary p_{l-o} /(MPa)	8.0
Elastic model E /(MPa)	2.0×10^3
Poisson's ratio ν	0.3
External stress σ_0 /(MPa)	20

3.2. Verification and analysis of calculation results

The evolution curves of volume fraction of fine particles, porosity, velocity of fluid and radial displacement at the inner boundary calculated according to the mathematical model in this paper are shown in figure 4 to figure 7 respectively, and the calculation results in this paper are compared with those in reference [29]. A comprehensive analysis of figure 4 to figure 7 shows that the evolution curves of volume fraction of fine particles, porosity, velocity of fluid, and radial displacement calculated by the mathematical model established in this paper are consistent to the results in reference [29]. Due to the difference between the porosity evolution equation, the permeability equation in this paper and those in reference [29], there is a certain error between the calculation results and those in reference [29]. However, the error is within the acceptable range. This also also verifies the correctness of the model in this paper.

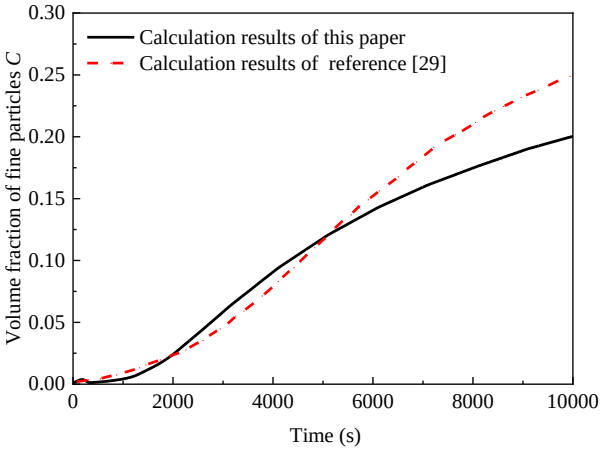

Figure 4. Evolution curves of the volume fraction of fine particles at inner boundary.

Preprints (www.preprints.org) | NOT PEER-REVIEWED | Posted: 23 September 2020 doi:10.20944/preprints202009.0527.v1

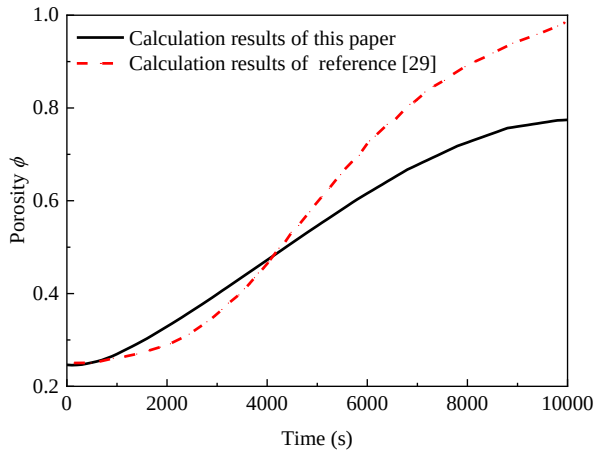

Figure 5. Evolution curves of porosity at inner boundary.

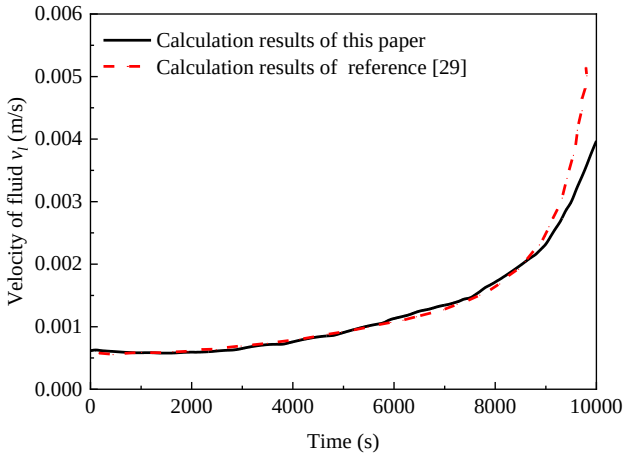

Figure 6. Evolution curves of the velocity of fluid at inner boundary.

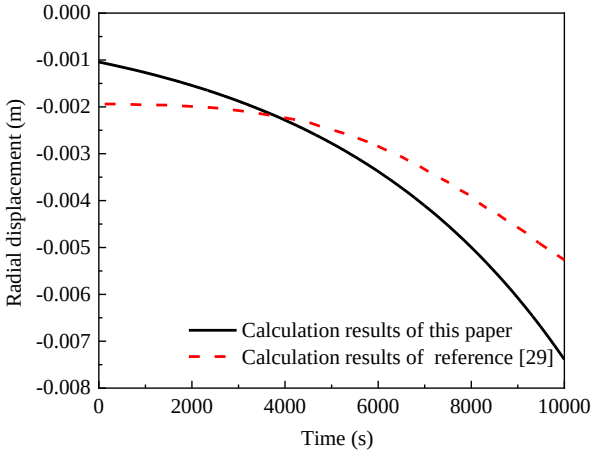

Figure 7. Evolution curves of the radial displacement at inner boundary.

4. Analysis of fluid-solid coupling characteristics of saturated coarse-grained filler considering the effect of fine particles migration

4.1. The establishment of numerical model

Preprints (www.preprints.org) | NOT PEER-REVIEWED | Posted: 23 September 2020 doi:10.20944/preprints202009.0527.v1

According to "Code for Design of Heavy Haul Railway (TB10625-2017)" [36] in China and referring to a typical section structure of the Shuo-huang Railway subgrade, a two-dimensional calculation model is established as shown in figure 8. The structure of the subgrade from top to bottom is as follows: surface layer of the subgrade (the thickness is 0.6m), bottom layer of the subgrade (the thickness is 1.9m). The slope gradient of the subgrade is 1:1.5. And the model sets four observation points, as shown in figure 8.

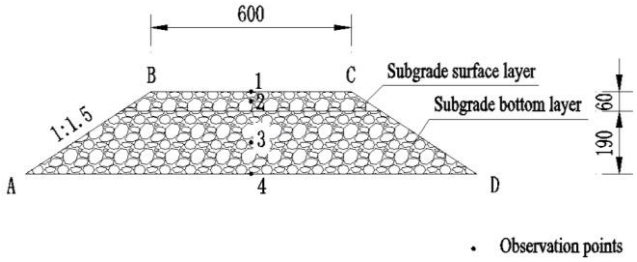

Figure 8. The fluid-solid two-phase coupling calculation model.

4.2. Mechanical parameters of subgrade filler

The filler of the subgrade is made of graded crushed stone. In order to analyze the influence of volume fraction of fine particles on the fluid-solid two-phase coupling characteristics of the filler, three different volume fraction of fine particles are selected, and the gradation of the graded crushed stone filler meet the requirements of the specification [37]. The physical parameters are shown in Table 2.

Table 2. Physical parameters for numerical calculation of subgrade model.

Parameter	Value
Initial porosity ϕ_0	0.33
Maximum porosity ϕ_{max}	0.50
Initial volume fraction of fine particles C_0	0.01/0.03/0.07
Critical volume fraction of fine particles C_{cr}	0.30
Initial permeability k_0 /(m²)	7.80×10^{-12}
The dynamic viscosity coefficient of the fluid μ_l /(Pa·s)	1.0×10^{-3}
The density of fluid ρ_l /(kg/m³)	1000
The density of fine particles ρ_p /(kg/m³)	2380
The erosion coefficient of fine particles ζ /(m^{-1})	1.0
Fluid pressure p_{l-in} /(kPa)	40.0
Elastic model E /(MPa)	120
Poisson's ratio ν	0.3

4.3. Boundary conditions and initial conditions

The initial conditions for the calculation model are: the pore water pressure is the hydrostatic pressure; the initial volume fraction of fine particles is 0.01, 0.03 and 0.07, respectively; the initial porosity of the subgrade is 0.3; and the initial displacement is 0.

It is assumed that the subgrade in the calculated area is saturated, and the dissipation path of pore water pressure is from bottom to top. The seepage boundary conditions for the calculation model are as follows: the lower boundary AD is the boundary of fluid pressure, and the fluid pressure at the boundary AD is set as 40 kPa according to the reference [1-3]. The fluid pressure at upper boundary BC is 0 kPa. And the slopes are usually protected, so AB and CD are assumed to be impermeable boundaries. The boundary conditions corresponding to the migration of fine particles

Preprints (www.preprints.org) | NOT PEER-REVIEWED | Posted: 23 September 2020 doi:10.20944/preprints202009.0527.v1

are as follows: the boundary AD is the inflow boundary for fine particles carried by the fluid, and the volume fraction of fine particles at the boundary AD is 0.01, 0.03 and 0.07, respectively. The upper boundary BC is the outflow boundary of fine particles. AB and CD are no flux boundary. The displacement boundary conditions are: the boundary AD is set as a fixed boundary, the remaining boundaries are free boundaries.

4.4. Calculation results and analysis

4.4.1. The variation of the volume fraction of fine particles

Figure 9 shows the evolution curves of the volume fraction of fine particles in saturated zone of railway subgrade. We can see from figure 9 that:

(1) With the increase of time, the volume fraction of fine particles at the observation points 1 to 3 first increased and then decreased: at initial moment, the volume fraction of fine particles was 0.01; when time is between 1100 minute to 1400 minute, the volume fraction of fine particles at different observation points in the subgrade reaches the maximum. Subsequently, the volume fraction of fine particles decreases gradually to about 0.01. This indicates that the fine particles are eroded by the fluid and migrated with the fluid, which lead the increase of the volume fraction of fine particles in the subgrade. As time goes by, fine particles are continuously eroded and flow out, leaving skeleton particles and larger particles in the subgrade which are difficult to migrate. Therefore, the volume fraction of fine particles decreases gradually.

(2) For observation points 1 to 3, the volume fraction of fine particles at observation point 3 firstly reaches the maximum value, and then the volume fraction of fine particles at observation point 2 and 1 successively reaches the maximum value. And the maximum volume fraction of the fine particles observed at point 1 is greater than that observed at point 2, the maximum volume fraction of the fine particles observed at point 2 is greater than that observed at point 3. The reasons is as follows: the seepage path of the fluid in the subgrade is from bottom to top, and the fluid erodes fine particles, then carries fine particles from the lower part of the subgrade to the upper part of the subgrade. Therefore, the volume fraction of fine particles at the observation point 3 first reaches its maximum value. However, the fluid continuously erodes fine particles and the eroded fine particles migrate to the upper part of the subgrade and flow out of the subgrade from the upper boundary. Therefore, the maximum volume fraction of fine particles at observation point 1 is larger than that at other observation points.

(3) As the observation point 4 is located at the lower boundary, it is the inflow boundary of fine particles, so the volume fraction of fine particles at the observation point 4 does not change.

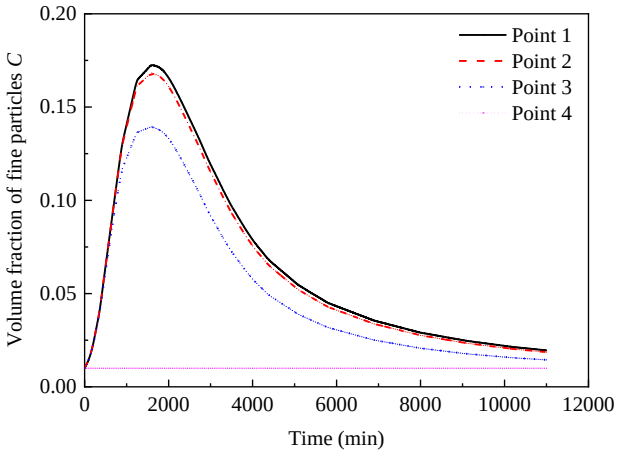

Figure 9. Evolution curves of the volume fraction of fine particles in saturated zone of railway subgrade.

4.4.2. The variation of porosity

Preprints (www.preprints.org) | NOT PEER-REVIEWED | Posted: 23 September 2020 doi:10.20944/preprints202009.0527.v1

Figure 10 shows the evolution curves of porosity in saturated zone of railway subgrade, in which subfigure (b) is the detailed curves for the curves in the box of subfigure (a). It can be seen from figure 10 that:

(1) The variation trend of porosity at the four observation points is the same: first, it increases slowly, then it increases rapidly to a certain value (about 0.5, i.e. the maximum porosity) and then it basically stable.

(2) For observation points 1 and 2, the time for the porosity to reach the maximum porosity is the same; for observation point 3, the time for the porosity to reach the maximum porosity is slightly later than that of observation points 1 and 2; while for observation point 4, it has the latest time to reaches the maximum porosity.

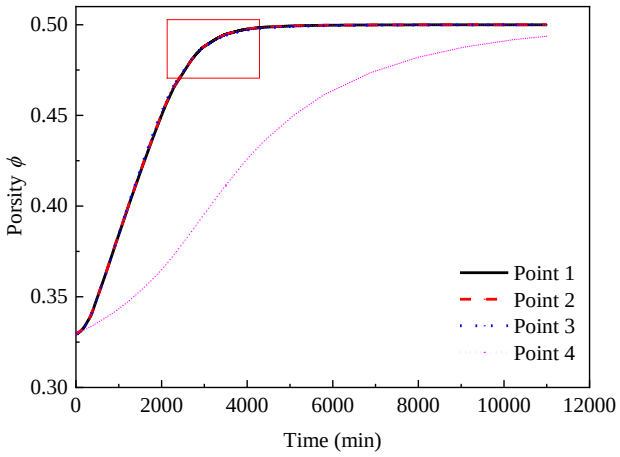

(**a**)

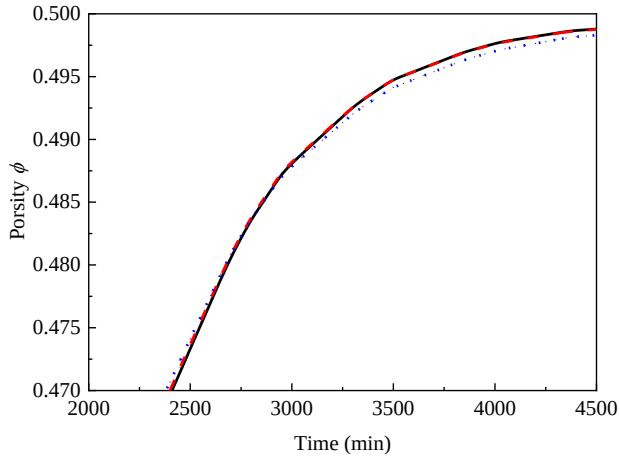

(**b**)

Figure 10. Evolution curves of porosity in saturated zone of railway subgrade: (a) Evolution curves of porosity; (b) A detailed diagram of the curves in a box in (a).

4.4.3. The variation of pore water pressure

Figure 11 shows the distribution cloud map of pore water pressure in saturated zone of railway subgrade, and figure 12 shows the evolution curve of pore water pressure at the observation points 3. From these two pictures we can see that:

(1) The pore water pressure at the lower boundary of the subgrade is 65 kPa, and the pore water pressure at the upper boundary of the subgrade is 0 kPa. The pore water pressure is evenly distributed from the bottom of the subgrade to the top of the subgrade.

Preprints (www.preprints.org) | NOT PEER-REVIEWED | Posted: 23 September 2020 doi:10.20944/preprints202009.0527.v1

(2) With the increase of time, the pore water pressure at point 3 shows a trend of first decreasing, then increasing and then decreasing, and finally remains stable, but the range of its increase or decrease is small. This is because: with the erosion and migration of fine particles in the subgrade, the porosity and permeability of each point inside the subgrade are different (see figure 10 and figure 14 for details), thus affecting the distribution of pore water pressure. Therefore, the pore water pressure at the same point is not constant.

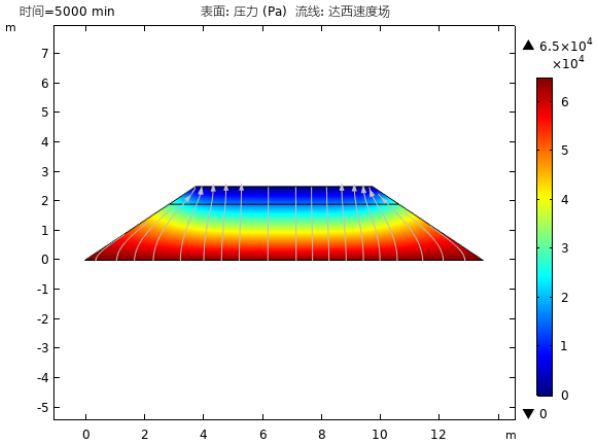

Figure 11. Distribution diagram of pore water pressure in saturated zone of railway subgrade (unit: Pa).

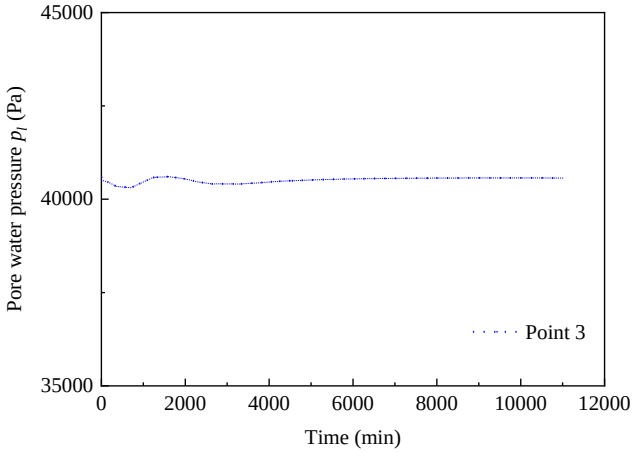

Figure 12. Evolution curve of pore water pressure in saturated zone of railway subgrade.

4.4.4. The variation of the velocity of fluid and the velocity of fine particles

Figure 13 shows the evolution curves of the velocity of fluid and the velocity of fine particles in saturated zone of railway subgrade. From figure 13 we can see:

(1) The variation trend of fluid velocity is basically the same as that of fine particles migration velocity, showing a trend of basically unchanged at first, then rapidly increasing, and finally tending to be stable.

(2) The velocity of fluid is always greater than the velocity of fine particles, and with the increase of fluid velocity, the velocity difference between these two is becoming more and more bigger. The reason is that: with the increases of the fluid velocity, the drag coefficient decreases, and the drag force of the fine particles is reduced, which hinders the movement of the fine particles to some extent.

Preprints (www.preprints.org) | NOT PEER-REVIEWED | Posted: 23 September 2020 doi:10.20944/preprints202009.0527.v1

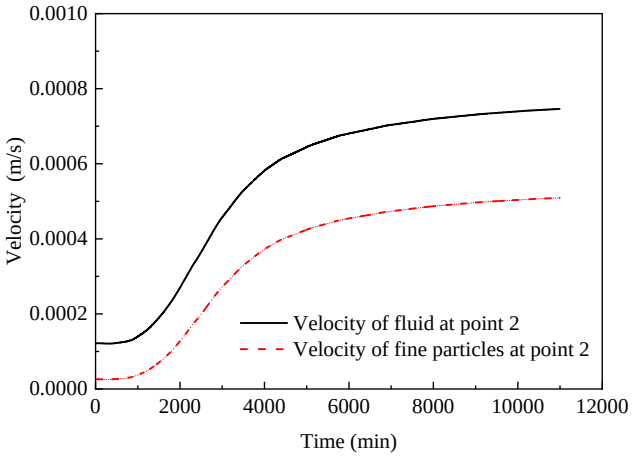

Figure 13. Evolution curves of velocity of fluid and fine particles in saturated zone of railway subgrade.

4.4.5. The variation of permeability

Figure 14 shows the evolution curves of permeability in saturated zone of railway subgrade. It can be seen from figure 14 that the permeability increases rapidly to the maximum after a relatively slow growth, and finally remains stable. For observation points 1~3, the maximum permeability is about 4.9×10^{-11} m^2, which is an increase of about 6.3 times higher than the initial permeability.

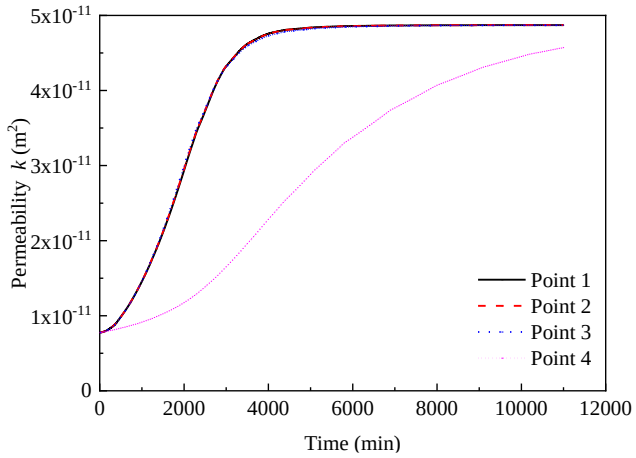

Figure 14. Evolution curves of permeability in saturated zone of railway subgrade.

4.4.6. Effect of initial volume fraction of fine particles on the evolution curves of the volume fraction of fine particles

Figure 15 shows the evolution curves of the volume fraction of fine particles with different initial fine particles volume fraction at point 2. From figure 15, we know that the larger the initial fine particles volume fraction is, the larger the maximum value of fine particles volume fraction is, and the shorter the time needed to reach the maximum value. Combined with equation (20), the larger the initial fine particles volume fraction is, the larger the mass rate of fine particles migration will be. Therefore, the shorter the time needed to reach the maximum fine particles volume fraction will be. It can be concluded that in practical engineering, the fine particles content in the filler of subgrade should be strictly controlled, and the fine particles content should be reduced as far as possible on the premise that the filler grade meets the requirements of the specification.

Preprints (www.preprints.org) | NOT PEER-REVIEWED | Posted: 23 September 2020 doi:10.20944/preprints202009.0527.v1

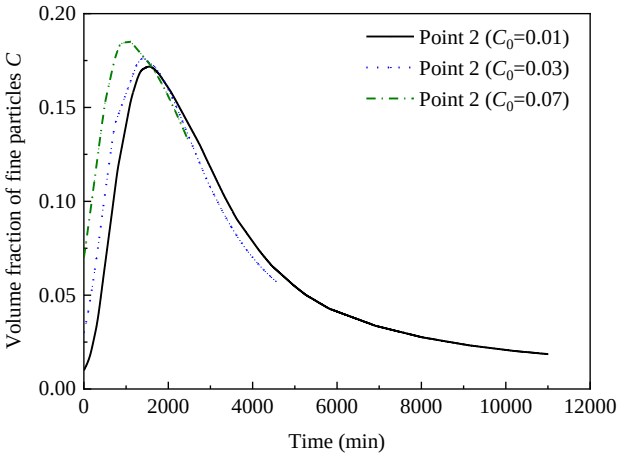

Figure 15. Evolution curves of the volume fraction of fine particles with different initial volume fraction of fine particles at point 2.

4.4.7. The variation of the vertical displacement

Figure 16 shows the contours of vertical displacement at the steady state of fluid seepage. We can see that the vertical displacement is distributed symmetrically on the central axis of the subgrade. At the same depth, the vertical displacement at the central axis of the subgrade is slightly larger than the vertical displacement at the edge of the subgrade.

Figure 17 shows the evolution curves of vertical displacement at different observation points in saturated zone of railway subgrade. It can be seen from figure 17 that the vertical displacement at different observation points increases first and then decreases slightly with the increase of time, and finally tends to be stable. The vertical displacement of the upper part of the subgrade is greater than that of the lower part of the subgrade. The final vertical displacement at observation point 1 is about 1.4mm, and the final displacement at observation point 3 is about 0.5mm.

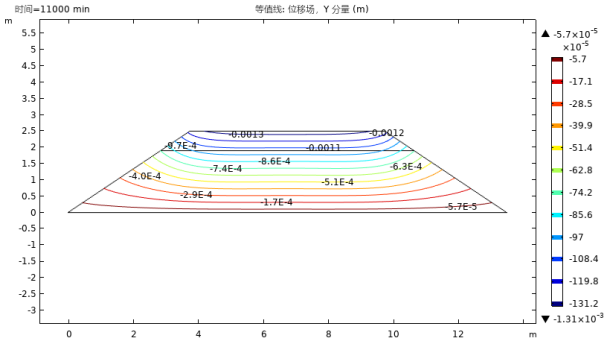

Figure 16. Contours of vertical displacement at the steady state of water flow (unit: m).

 doi:10.20944/preprints202009.0527.v1

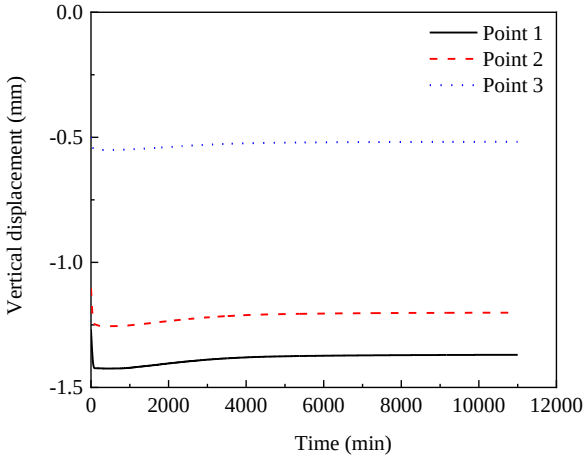

Figure 17. Evolution curves of the vertical displacement in saturated zone of railway subgrade.

5. Conclusions

Based on the theory of two-phase seepage, the theory of porous media seepage, and the principle of effective stress in porous media, a two-phase fluid-solid coupling mathematical model in local-saturated zone of subgrade considering the effect of fine particles migration is established. The mathematical model is numerically calculated with the software COMSOL Multiphysics®, the two-phase seepage characteristics in local-saturated zone of the subgrade and the deformation characteristics of the solid skeleton are studied, and the following conclusions are obtained:

(1) Under the action of fluid seepage, the erosion and migration of the fine particles in local-saturated zone of subgrade gradually occurred, and the volume fraction of fine particles increased with the increase of time, and as time goes on, only skeleton particles and particles with large sizes are left in the subgrade, the volume fraction of fine particles gradually decreases to the initial value. The constant erosion of fine particles inside the subgrade and the constant migration of fine particles with fluid from the lower part of the subgrade to the upper part of the subgrade cause that the volume fraction of fine particles in the upper part of the subgrade is larger than that in the lower part of the subgrade at the same time.

(2) With the increase of time, the porosity, the velocity of fluid, the velocity of fine particles, and the permeability of the subgrade show the trend of first increasing and then stabilizing; the pore water pressure in the subgrade has no significant changes with time.

(3) The vertical displacement is distributed symmetrically on the central axis of the subgrade. With the increase of time, the vertical displacement increase first and then decrease slightly and finally tend to be stable.

(4) For a filler with a larger initial volume fraction of fine particles, the maximum value of the volume fraction of fine particles in the subgrade caused by fluid seepage is larger, and the time required to reach the maximum value is shorter. It can be concluded that in actual engineering, the volume fraction of fine particles in the subgrade filler should be minimized on the premise that the filler gradation meets the requirements of the specification.

The main purpose of this research is to explore the characteristics of the two-phase seepage and the deformation of solid skeleton in local-saturated zone of the subgrade considering the effect of fine particles migration, in order to explain the internal mechanism of the mud pumping disease. Therefore, the dynamic characteristics of the subgrade filler and the fluid-solid two-phase seepage characteristics considering the effect of fine particles migration and sedimentation under train load have more practical engineering significance, which will also be the focus of the next research.

Author Contributions: Conceptualization, Y.D. and Y.J.; methodology, J.Z., X.C. and X.W.; software, F.M.; validation, Y.D. and Y.J.; formal analysis, Y.D.; investigation, Y.J.; resources, J.Z.; data curation, Y.J.; writing—original draft preparation, Y.D.; writing—review and editing, Y.D.; visualization, Y.D.; supervision and project administration, J.Z.; funding acquisition, X.C.. All authors have read and agreed to the published version of the manuscript.

Funding: The research was funded by the National Natural Science Foundation of China under grant number CNNSF 51608533. The laboratory tests were partially supported by the China Railway Corporation Science and the Technology Development Project under grant number 2017G008-A.

Conflicts of Interest: The authors declare no conflict of interest. The funders had no role in the design of the study; in the collection, analyses, or interpretation of data; in the writing of the manuscript, or in the decision to publish the results.

References

1. T. V. Duong, Y. J. Cui, A. M. Tang. et al. Physical model for studying the migration of fine particles in the railway substructure[J]. Geotechnical Testing Journal, 2014, 5(37): 895-906.
2. T. V. Duong, Y. J. Cui, A. M. Tang, et al. Investigating the mud pumping and interlayer creation phenomena in railway sub-structure[J]. Engineering Geology, 2014, 171:45-58.
3. A. Abeywickrama, B. Indraratna, and C. Rujikiatkamjorn. Excess pore-water pressure generation and mud pumping in railways under cyclic loading [J]. Geotechnics for Transportation Infrastructure, 2019, 28:371-383.
4. I. Alobaidi, D. J. Hoare. The development of pore water pressure at the subgrade-subbase interface of a highway pavement and its effect on pumping of fines [J]. Geotextiles & Geomembranes, 1996, 14(2):111-135.
5. I. Alobaidi, D. J. Hoare. Mechanisms of pumping at the subgrade-subbase interface of highway pavements[J] Geosynthetics International,1999, 6(4):241-259.
6. J. F. Schijven, S. M. Hassanizadeh. Removal of viruses by soil passage: overview of modeling, processes, and parameters[J]. C R C Critical Reviews in Environmental Control, 2000, 30(1):49-127.
7. R. Kretzschmar, K. Barmettler, D. Grolimund, et al. Experimental determination of colloid deposition rates and collision efficiencies in natural porous media[J]. Water Resources Research, 1997, 33(5):1129-1137.
8. S. A. Bradford, J. Simunek, M. Bettahar, et al. Modeling colloid attachment, straining, and exclusion in saturated porous media[J]. Environmental Science & Technology, 2003, 37(10):2242-2250.
9. J. Zhao, Q. S. Liu, C. Y. Zhang. Establishment of particle transport model in water source heat pump of physical clogging reinjection well[J]. Rock and Soil Mechanics, 2013(11): 3249-3253.
10. B. Kermani, M. Xiao, S. M. Stoffels, et al. Measuring the migration of subgrade fine particles into subbase using scaled accelerated flexible pavement testing – a laboratory study[J]. Road Materials and Pavement Design, 2019, 1(20): 36-57.
11. D. Liu, P. R. Johnson, M. Elimelech. Colloid deposition dynamics in flow-through porous media: role of electrolyte concentration[J]. Environmental Science & Technology, 1995, 29(12):2963-2973.
12. J. P. Herzig, D. M. Leclerc, P. L. Goff. Flow of suspensions through porous media-application to deep filtration[J]. Industrial & Engineering Chemistry, 1970, 62(5):8-35.
13. X. Yin, B. Gao, L. Q. Ma, et al. Colloid-facilitated Pb transport in two shooting-range soils in Florida[J]. Journal of Hazardous Materials, 2010, 177(1-3):620-625.
14. B. Bai, P. Y. Zhang, X. M. Song, et al. Transport processes of suspended particles in saturated porous media by column seepage tests[J]. Chinese Journal of Geotechnical Engineering, 2015, 37(10):1786-1793.
15. P. Y. Zhang, B. Bai, S. C. Jiang. Coupled effects of hydrodynamic forces and pore structure on suspended particle transport and deposition in a saturated porous medium[J]. Rock and Soil Mechanics, 2016, 37(5): 1307-1316.
16. Q. S. Liu, X. Z. Cui, C. Y. Zhang, et al. Effects of particle size on characteristics of transportation and deposition of suspended particles in porous media[J]. Chinese Journal of Geotechnical Engineering, 2014, 36(10):1777-1783.
17. K. Terzaghi． Theoretical soil mechanics[M]. Wiley, New York, 1943.
18. M. A. Biot. General Theory of three-dimensional consolidation[J]. J.Appl.Phys, 1941, (12): 155-164.
19. M. A. Biot. Theory of elastic waves in a fluid-saturated porous solid[J]. J. Acous. Soc. Americ, 1956, (28): 168-191.
20. O. C. Zienkiewics, T. Shiomi. Dynamic behavior of saturated porous media: the generalized Biot formulation and its numerical solution [J]. Int. J. Num. and Analy: Mech. in Geomech, 1984, 8: 71-96.
21. W. Z. Savage, W. A. Braddock. A model for hydrostatic consolidation of Pierre shale[J]. International Journal of Rock Mechanics & Mining science & Geomechanics Abstracts, 1982, 28(5):345-354.
22. R. W. Zimmerman. Coupling in poroelasticity and Ther-moelasti city[J]. International Journal of Rock Mechanics&Mining Sciences, 2000, 37(1):79-87.
23. Z. J. Shen. Calculation of consolidation deformation of soft soil foundation by finite element method[J]. Hydro-Science and Engineering, 1977(1):9-25.

24. Y. Liang, L. Chen, J. S. Chen. Mathematical model for piping development considering fluid-solid interaction[J]. Chinese Journal of Geotechnical Engineering, 2011, 33(8): 1265-1270.
25. Z. Zhou, H. L. Fu, B. C. Liu, et al. Artificial rainfall tests on a well-instrumented soil-rock-mixture slope[J]. Rock and Soil Mechanics, 2007, 28(7):1391 -1396.
26. W. Chen, W. S. Pei, S. Y. Li, et al. Numerical simulation and engineering application of solid-liquid coupled model for saturated porous media[J]. Chinese Journal of Rock Mechanics and Engineering, 2013(z2):3346-3354.
27. R. Sakthivadivel. Theory and mechanism of filtration of non-colloidal fines through a porous medium[M]. HEL 15-5,6,7, University of California, Berkekey, 1966.
28. R. Sakthivadivel, S. Irmay. A review of filtration theories[M]. HEL 15-4, University of California, Berkekey,1966.
29. M. Stavropoulou, P. Papanastasiou, I. Vardoulakis. Coupled wellbore erosion and stability analysis[J]. International Journal for Numerical & Analytical Methods in Geomechanics, 1998, 22(9):749-769.
30. I. Vardoulakis, M. Stavropoulou, R. Papanastasiou. Hydro-mechanical aspects of the sand production problem[J]. transport in porous media, 1996, 22(2):225-244.
31. P. Sharma, M. Flury, E. D. Mattson. Studying colloid transport in porous media using a geocentrifuge[J]. Water Resources Research, 2008, 44(7):767-768.
32. B. Berkowitz, A. Cortis, M. Dentz, et al. Modeling non-Fickian transport in geological formations as a continuous time random walk, Rev. Geophys.2006, 44.
33. R. Kretzschmar, K. Barmettler, D. Grolimund, et al. Experimental determination of colloid deposition rates and collision efficiencies in natural porous media[J]. Water Resources Research, 1997, 33(5):1129-1137.
34. N. Massei, M. Lacroix, H. Q. Wang, et al. Transport of particulate material and dissolved tracer in a highly permeable porous medium: comparison of the transfer parameters[J]. Journal of Contaminant Hydrology, 2002, 57(1-2):21-39.
35. Z. J. Luo, H. Z. Li, Y. L. Fu. Numerical simulation of groundwater seepage and land subsidence control in quaternary loose sediments[M]. Science Press, 2009.
36. TB10625-2017, Code for Design of Heavy Haul Railway[S]. Beijing: China Railway Publishing House, 2017.
37. TB10001-2016, Code for Design of Railway Earth Structure[S]. Beijing: China Railway Publishing House, 2016.